Stiffness model of machine tool supports using contact stiffness

Daisuke Kono, Takahiro Inagaki, Atsushi Matsubara, Iwao Yamaji

Dept. of Micro Engineering, Graduate School of Engineering, Kyoto University
Yoshida-honmachi, Sakyo-ku, Kyoto 606-8501, Japan
Email: kono@prec.kyoto-u.ac.jp
Phone: +81-75-753-5226
Fax: +81-75-753-5226

Abstract

The stiffness of machine tool supports should be properly designed for reducing both the ground disturbance vibration and the drive disturbance vibration. However, the stiffness cannot be easily calculated from the geometry and material properties of the support. In this paper, a 3D stiffness model of a machine tool support is proposed using contact stiffness. The stiffness in each direction is assumed to be determined by the contact stiffness at the interfaces and the bulk stiffnesses of the supports and the floor. The contact stiffness model proposed by Shimizu et al. is expanded to determine the contact stiffness in the normal and tangential directions of an interface. In the proposed model, the contact stiffness is obtained by multiplying the unit contact stiffness by the real contact area. The contact stiffness of concrete is experimentally investigated to estimate the stiffness between machine tool supports and the floor, and it was observed to be the primary determinant of the stiffness of interfaces between metal and concrete. Moreover, the unit contact stiffness of concrete is discovered to be less than 1/10 of those of the metals that were used for the study. The natural frequency and vibration mode shape of a model machine tool bed are also experimentally measured and used to verify the proposed stiffness model. The comparison of the results obtained from the two procedures shows that the natural frequency and vibration mode shape of a machine tool bed can be predicted using the proposed stiffness model.

Keywords: stiffness model, support stiffness, contact stiffness, concrete, machine tool

Nomenclature

W	normal load
W_{pre}	normal preload
W_v	variable normal load
F	tangential load
k_n	normal contact stiffness
k_t	tangential contact stiffness
k_{nmc}	normal contact stiffness between the middle specimen and the lower specimen of the metal–concrete specimen set
k_{nmm}	normal contact stiffness between the middle specimen and the lower specimen of the metal–metal specimen set
δk_n	unit normal contact stiffness
δk_t	unit tangential contact stiffness
δk_{nc}	unit normal contact stiffness of concrete
δk_{nm}	unit normal contact stiffness of metal
δk_{tc}	unit tangential contact stiffness of concrete
δk_{n1}, δk_{n2}	unit normal contact stiffnesses of materials 1 and 2
δk_{t1}, δk_{t2}	unit tangential contact stiffnesses of materials 1 and 2
i	subscript representing normal and tangential directions
K_{nl}	normal stiffness of the lower specimen
K_{nu}	normal stiffness of the upper specimen
K_{nmc}	normal stiffness between the upper specimen and the lower specimens of the metal–concrete specimen set
K_{nmm}	normal stiffness between the upper specimen and the lower specimen of the metal–metal specimen set
p_m	yield pressure
A_r	real contact area
A_{rmc}	real contact area between the middle specimen and the lower specimen of the metal–concrete specimen set
A_{rmm}	real contact area between the middle specimen and the lower specimen of the metal–metal specimen set
d_{nl}	normal displacement of the lower specimen
d_{nu}	normal displacement of the upper specimen

1. Introduction

There has been a demand for higher efficiency in high-precision machining in recent times. Vibration of machine tools, such as those that result in the relative displacement of the tool and the table, pose a huge challenge to high-precision machining. Machine tool vibrations are classified into two types, namely, (1) ground disturbance vibration transmitted by the floor on which the machine is installed, and (2) drive disturbance vibration generated by the feed drives. Both types of vibrations are greatly determined by the stiffness of the machine tool supports.

Ground disturbance vibration can be reduced by using soft supports such as rubbers and air springs [1-4]. Unfortunately, soft supports also cause the entire machine to rock, thereby increasing the drive disturbance vibration [1]. The stiffness of machine tool supports should therefore be designed by taking into consideration the amplitudes of both types of vibration.

However, owing to the fact that the factors that determine the stiffness of machine tool supports have not been clarified, they have only been designed empirically by most machine tool builders. Moreover, since the stiffness of the support cannot be easily calculated from its geometry and material properties, it would have to be modeled on the basis of other factors to aid systematic design.

Some studies have shown that the stiffness at the interface (contact stiffness) of a support significantly affects the overall stiffness of the support [5,6]. Hoshi particularly noted that contact stiffness with the concrete floor is the most important factor that determines the stiffness of a support [5].

There have actually been many studies on contact stiffness. Theoretical models have been proposed on the basis of the Hertz theory, and the governing equation of the contact stiffness were derived [7,8]. The contact stiffness has also been measured in directions normal and tangential to the interface to verify proposed models [9-11]. Furthermore, the influence of surface topography on contact stiffness has been investigated [12]. While these experimental studies examined contact stiffness between the same type of materials (mostly steel), machine tool supports usually involve contact between different types of materials such as cast iron, steel, and concrete. The contact stiffness between metals and concrete is particularly of interest because concrete is the usual material used for the floor of workshops and factories. Shimizu et al. proposed a simple model of the contact stiffness at the interface of different materials and measured the stiffness normal to the interface for several combinations of materials [13].

In this paper, a model of the stiffness of a machine tool support is proposed on the basis of Shimizu et al.'s contact stiffness model. The model is then used to estimate the contact stiffness of interfaces between several metals and concrete in directions normal and tangential to the interface. Finally, the estimates of the proposed model are experimentally verified using a small model of a machine tool bed.

2. Model of machine tool supports and contact stiffness

2.1 Stiffness model of machine tool supports

Figure 1 shows examples of machine tool supports. Medium- and small-sized machine tools are generally mounted on concrete floors with the aid of screw jacks or leveling blocks. Such height adjustment supports are used to ensure that the machine is leveled when installed.

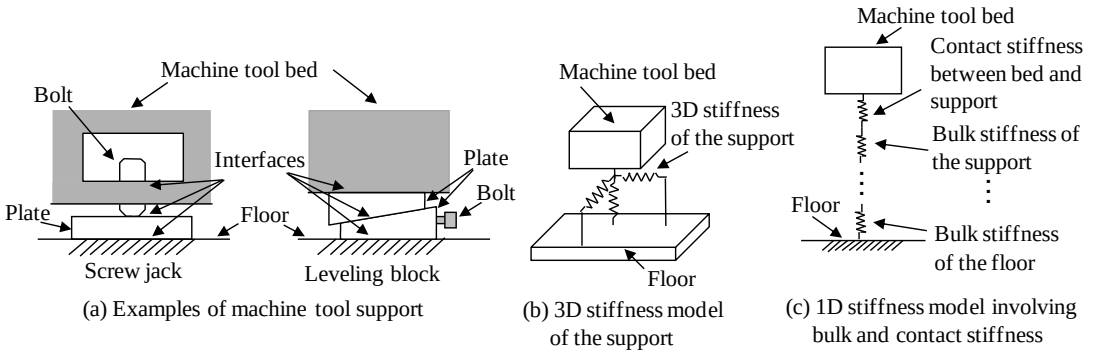

Fig. 1 Machine tool support and its model

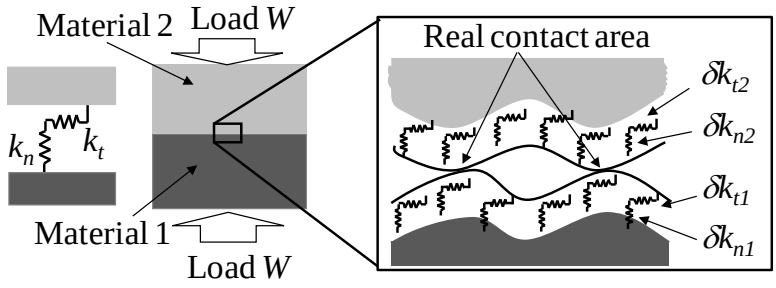

(a) Contact stiffness in the support

(b) Unit contact stiffness model at the interface

Fig. 2 Model of contact stiffness

In this study, the stiffness of one support is modeled in 3D as shown in Fig. 1(b). The stiffness in each direction is assumed to be determined by the contact stiffness at the interface and the bulk stiffnesses of the support and floor. Hence, the stiffness in each direction is modeled by the bulk stiffness and the contact stiffness connected in series, as shown in Fig. 1(c). The bulk stiffness can be calculated from the modulus of elasticity and the geometry of the support. In this study, the contact stiffness is treated as a linear stiffness. A model of the contact stiffness is described in the following section.

2.2 Model of contact stiffness

The contact stiffness model proposed by Shimizu et al. [13] is modified here. Figure 2(a) shows a schematic of two materials in contact at the machine tool support. The load W acts on the interface; k_n and k_t are the contact stiffnesses in directions normal and tangential to the interface, respectively.

In Shimizu et al.'s model, k_n is considered to be the contact stiffness associated with a series of coupled springs spread over the interface. In this study, this model is expanded to obtain k_t as shown in Fig. 2(b). δk_{n1} and δk_{n2} are the normal contact stiffnesses per unit real contact area (unit normal contact stiffness) of materials 1 and 2, respectively; and δk_{t1} and δk_{t2} are the tangential contact stiffnesses per unit real contact area (unit tangential contact stiffness). The real contact area is determined by the contacting roughness asperity of the interface. k_i ($i = n, t$) is given by

$$k_i = \frac{\delta k_{i1}\delta k_{i2}}{(\delta k_{i1} + \delta k_{i2})} A_r \tag{1}$$

where A_r is the real contact area and the subscript i represents the normal or tangential direction. A_r is given by

$$A_r = \frac{W}{p_m} \tag{2}$$

where p_m is the lower of the yield pressures of materials 1 and 2 [14]. In this study, the yield pressure is assumed to be equal to the Vickers hardness.

From Eq.1 and Eq.2, we see that k_i is a nonlinear stiffness dependent on W. This is because the plastic deformation of the interface increases A_r. In the machine tool support, W is determined by the steady load corresponding to the weight of the machine tool and the variable load corresponding to the drive disturbance caused by the drives of the machine. Considering that the steady load is generally much greater than the variable load, the latter can be neglected and the contact stiffness is treated as a linear stiffness.

3. Estimation of unit contact stiffness for concrete

δk_n and δk_t are required to estimate the contact stiffness using the proposed model. In our previous work, δk_n and δk_t were given for several metals usually used for machine tool support [15]. In this study, δk_n and δk_t are experimentally measured for concrete.

3.1 Estimation method

Figure 3 shows the specimen set used for the measurement. The set comprised upper, middle, and lower specimens. The contact stiffness values between the middle specimen and the other two specimens can be measured at two interfaces. Different materials are used for the specimens in order to estimate the contact stiffness for different combinations of materials. The dimensions of the middle specimen were chosen such that the real contact area would be less than the nominal contact area under a normal load of 10 kN, which was considered typical of the load on the supports of a small machine tool.

The contact stiffness of the specimen set is obtained from the stiffness between the

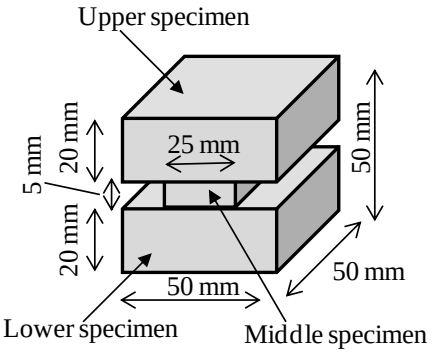

Fig. 3 Specimen set used in the measurement

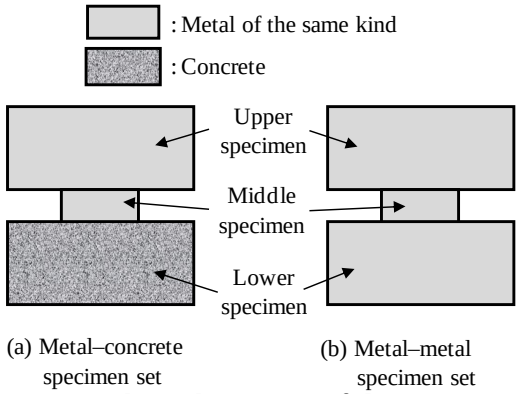

Fig. 4 Material combinations of the specimen set

upper and lower specimens. As described in the following section, the stiffness between the upper specimen and the lower specimen consists of contact stiffness and bulk stiffness. The contact stiffness is typically determined by comparing the stiffness of the specimen set with that of a monolithic specimen that has no interface [15]. However, because it is difficult to produce a monolithic specimen from brittle concrete, a different method is used in this study.

The different combinations of the specimen materials that are used are shown in Fig. 4. Measurements are taken for a metal–concrete specimen set in which the lower specimen is made of concrete (Fig. 4(a)) and a metal–metal specimen set comprising specimens of the same kind of metal (Fig. 4(b)). Measurement results for these specimen sets are compared to determine the contact stiffness between the middle specimen and the lower specimen of the metal–concrete specimen set. The details of the procedure used to obtain δk_n are given below.

3.1.1 Measurement with metal–concrete specimen set

The normal stiffness K_{nmc} between the upper and lower specimens of the metal–concrete specimen set is measured. A schematic of the measurement is shown in Fig. 5. A steady normal load W_{pre} is preloaded on the upper specimen and the normal displacements d_{nl} and d_{nu} of the lower and upper specimens are measured while the normal load W_v is cyclically loaded and unloaded on the upper specimen. The stiffness K_{nl} of the lower specimen is calculated from the relationship between d_{nl} and W_v. The relationship between d_{nl} and W_v during the unloading is used to eliminate the effect of plastic deformation of the specimens. Similarly, the stiffness K_{nu} of the upper specimen is calculated from d_{nu} and W_v. K_{nmc} is then calculated using

$$K_{nmc} = \frac{K_{nu}K_{nl}}{K_{nl} - K_{nu}} \tag{3}$$

3.1.2 Measurement with metal–metal specimen set

K_{nmc} is the resultant stiffness of the contact stiffness at the two interfaces and the bulk stiffness of the specimens. Therefore, the stiffness K_{nmm} between the upper and lower specimens of the metal–metal specimen set is obtained to determine the contact stiffness between the middle specimen and the lower specimen of both specimen sets. A similar method as explained in Section 3.1.1 is used to obtain K_{nmm}.

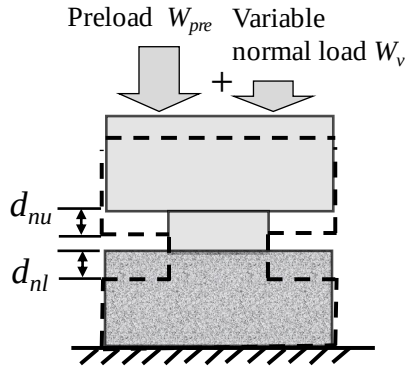

Fig. 5 Schematic of measurement in the normal direction

3.1.3 Calculation of contact stiffness

The contact stiffness between the middle specimen and the lower specimen of both specimen sets is determined using the following relation:

$$\frac{1}{K_{nmc}} - \frac{1}{K_{nmm}} = \frac{1}{k_{nmc}} - \frac{1}{k_{nmm}} \tag{4}$$

where k_{nmc} and k_{nmm} are the normal contact stiffnesses between the middle specimen and the lower specimen of the metal–concrete and the metal–metal specimen sets, respectively. By substituting Eq.1 into Eq.4, we get the unit normal contact stiffness δk_{nc} of concrete as

$$\delta k_{nc} = \frac{1}{A_{rmc}} \left(\frac{1}{K_{nmc}} - \frac{1}{K_{nmm}} + \frac{2}{\delta k_{nm} \cdot A_{rmm}} - \frac{1}{\delta k_{nm} \cdot A_{rmc}} \right)^{-1} \tag{5}$$

where δk_{nm} is the unit normal contact stiffness of the metal, A_{rmc} is the real contact area between the middle specimen and the lower specimen of the metal–concrete specimen set, and A_{rmm} is the real contact area between the middle specimen and the lower specimen of the metal–metal specimen set. Strictly speaking, δk_{nc} determined from this experiment include the difference between the bulk stiffnesses of concrete and metal.

The unit tangential contact stiffness δk_{tc} of concrete is obtained through a procedure similar to that described in Sections 3.1.1–3.1.3. W_{pre} is initially preloaded on the upper specimen, but a tangential load F is loaded instead of W_v. The tangential displacements of the upper and lower specimens are measured.

3.2 Measurement device and experimental conditions

Figure 6 shows the setup of the experiment. The specimen is mounted on the compression testing machine (SHIMADZU) to apply a normal load. The normal load is applied through a steel ball to minimize the tilting of the specimen. The normal load is measured using a load cell installed on the testing machine.

In the measurement in the normal direction shown in Fig. 6(a), the normal displacement of the specimen is measured with an electric micrometer mounted with a

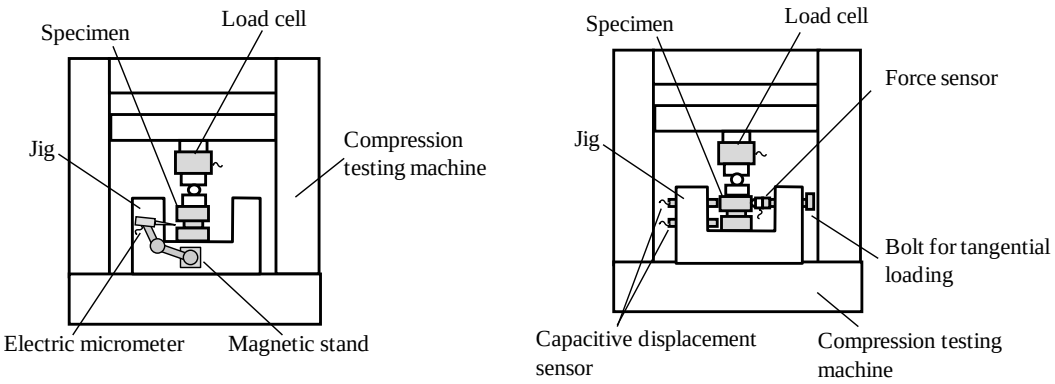

(a) Measurement in the normal direction

(b) Measurement in the tangential direction

Fig. 6 Schematic of measurement setup

Table 1 Specifications of measuring instruments

Force sensor	Measuring range	±5 kN
	Accuracy	±1%
Load cell	Measuring range	±10 kN
	Accuracy	±0.02%
Capacitive displacement sensor	Measuring range	±250 μm
	Accuracy	±1%

Table 2 Specifications of specimens

Material	S50C	SS400	FC250	Concrete
Longitudinal elastic modulus GPa	205	206	127	25–40
Measured Vickers hardness kgf/mm^2	230	180	230	56 (mortar) 1470 (gravel)
Measured surface roughness Rz μm	4.0	1.1	1.5	3.6
Unit normal contact stiffness δk_n N/mm/mm^2	1.4×10^7	1.8×10^7	1.0×10^7	Not measured
Unit tangential contact stiffness δk_t N/mm/mm^2	1.6×10^6	1.6×10^6	2.0×10^6	Not measured

magnetic stand on the jig below the specimen. The stiffness is measured on the left and right sides of the middle specimen and the average value is used to minimize the effect of tilting of the specimen.

In the measurement in the tangential direction shown in Fig. 6(b), a tangential load is applied through a bolt, which is measured using a force sensor (Kistler). The tangential displacement of the specimen is measured with a capacitive displacement sensor (Lion Precision). Block gauges are fixed to the specimens as targets for the sensor. The specifications of the measuring instruments are listed in Table 1.

Carbon steel S50C, low alloy steel SS400, and cast iron FC250 are used as the metal specimens. Their specifications are given in Table 2. The values of δk_n and δk_t obtained in a previous work [15] are also given for the three metal specimens. The surface roughness of the specimens was measured with a contact-type surface roughness measuring machine. The surface of the concrete specimen was ground and polished. Since the Vickers hardness of the mortar in the concrete specimen was lower than that of the gravel in it, A_{rmc} is calculated using the Vickers hardness of mortar. All the surfaces of the specimens are cleaned with ethanol in preparation for the experiment.

To eliminate the effect of plastic deformation, a normal load of 10 kN is applied on the specimens for about 10 min. before measurements are performed. While measuring in the normal direction, a W_{pre} of 9 kN and W_v of ±1 kN are applied on the specimen sets. While measuring in the tangential direction, the maximum value of F is set to 1 kN for a W_{pre} of 10 kN. The cyclic process of loading and unloading are repeated five times. The sampling frequency of the measurement is set to 100 Hz.

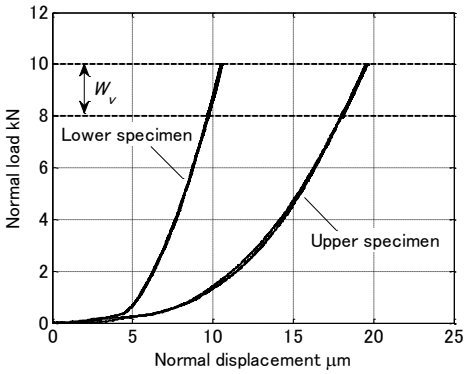

Fig.7 Relationship between normal displacement and load for the metal–concrete specimen set. The material of the metal specimen is S50C.

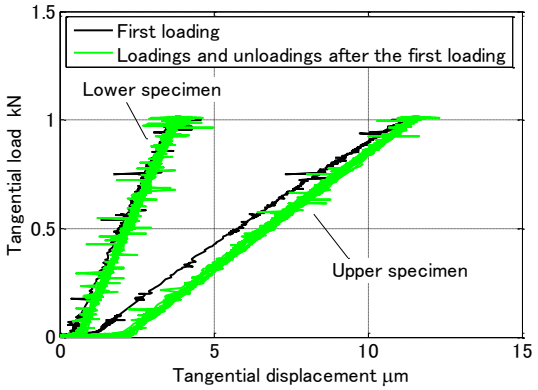

Fig.8 Relationship between tangential displacement and load for the metal–concrete specimen set. The material of the metal specimen is S50C.

3.3 Experimental result

Figure 7 shows the relationship between the normal load, comprising W_{pre} and W_v, and the normal displacement of the left side of the metal–concrete specimen set, in which S50C is the metal. A nonlinear relationship is observed in all the relationships for preloading. The nonlinearity is due to the increase in the real contact area resulting from the elastic deformation of the interface. Thornley et al. also reported a similar relationship in their article [12]. Because the relationship is approximately linear for values of W_v, K_{nu} and K_{nl} were obtained by the least-squares fitting method.

Figure 8 shows the relationship between the tangential load and the tangential displacement for the metal–concrete specimen set. A linear relationship is observed here because the real contact area did not change when loading in the tangential direction. The tangential stiffnesses of the upper and lower specimens were therefore also obtained by the least-squares fitting method. As can be observed, the curve of the first loading of the upper specimen differs from those of subsequent loading and unloading, which is the result of the plastic deformation of the interface after the first loading. Although the normal preload that primarily determined the real contact area was constant, there was still a small increase in the contact area as a result of the tangential load. Tangential displacements of 2 μm and 0.5 μm resulting from plastic deformation are observed in the upper and lower specimens, respectively.

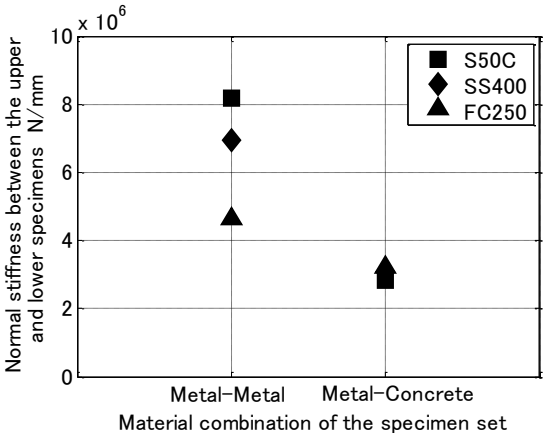

Fig. 9 Comparison of normal stiffness between the upper and lower specimens

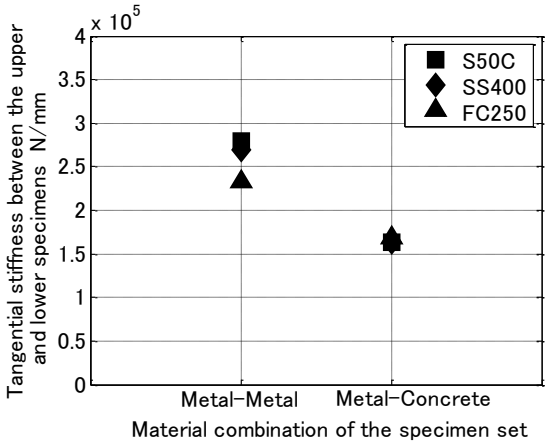

Fig. 10 Comparison of tangential stiffness between the upper and lower specimens

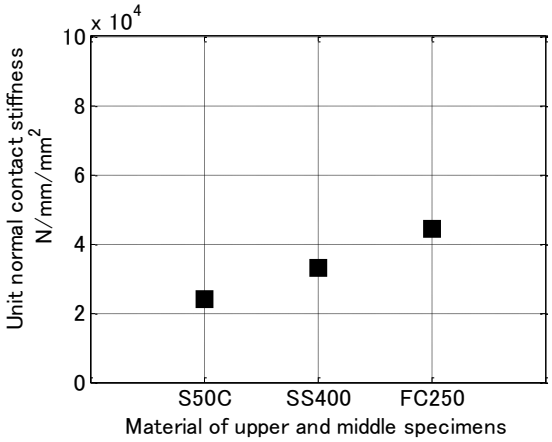

Fig. 11 Unit normal contact stiffness of concrete

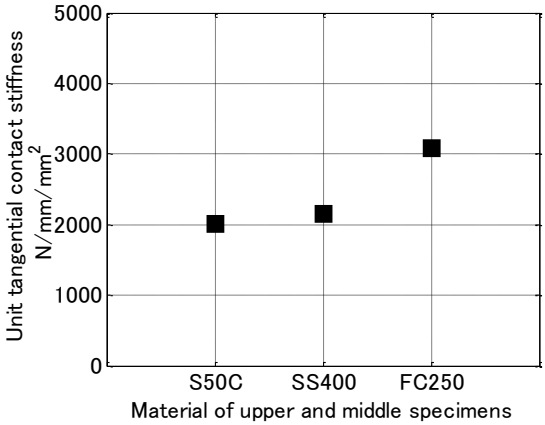

Fig. 12 Unit tangential contact stiffness of concrete

Results similar to those shown in Figs. 7 and 8 were also observed when SS400 and FC250 were used for the metal specimen. These results were used to determine the stiffness between the upper and lower specimens for all the specimen sets. Figure 9 shows a comparison of the normal stiffnesses K_{nmm} and K_{nmc}, and Fig. 10 shows a comparison of the tangential stiffnesses between the upper and lower specimens. In both figures, the stiffness of the metal–concrete specimen set is observed to be lower than those of the metal–metal specimen sets. Moreover, the stiffness is almost the same when different materials were used for the upper and middle specimens of the metal–concrete specimen set. This indicates that the stiffness of a metal–concrete interface is primarily determined by concrete.

Figures 11 and 12 show the values of δk_{nc} and δk_{tc}, respectively, for the metal–concrete specimens. As is the case with the metals listed in Table 2, the values of δk_{nc} is about 10 times those of δk_{tc}, although the respective values are smaller than those of the metals. The values of δk_{nc} are in the range of 1/67–1/23 of those of the metals, while those of δk_{tc} are in the range of 1/79–1/68. The large difference between the observed stiffness of concrete and those of metals can be partly attributed to the fact that the values of δk_{nc} and δk_{tc} obtained from this experiment were affected by the difference

between the bulk stiffness of concrete and that of the interfacing metal. As a result, δk_{nc} and δk_{tc} are slightly higher when the lower specimen is FC250, since its elastic modulus is lower than those of S50C and SS400.

4. Experimental verification of the stiffness model

4.1 Model of a machine tool bed used for verification

An experiment is performed to verify the stiffness model proposed above. The natural frequency and vibration mode shape of a small model of a machine tool bed are estimated and compared with experimental results.

Figure 13 shows the machine tool bed model, a block of FC250, that was used for the experiment. The mass of the block is about 23 kg. The block is freely mounted on the concrete floor atop three cylindrical supports made of SS400. The supports are positioned as illustrated in Fig. 14. To simplify the calculation of the normal preload on each, the supports are positioned symmetrically about the center of gravity of the machine tool model.

All the interfaces of the model and floor are ground and cleaned with a cleaning fluid. The surface roughnesses of the interfaces were measured by a contact type surface roughness measuring machine (Mitutoyo). In particular, the surface roughness of the floor was measured by a portable type surface roughness measuring machine. The surface roughness of the bed was estimated from the measurement with a plate of FC250 ground similarly to the bed because the bed is too large for the measuring machine. The surface roughnesses of the support and bed are 3.9 μmRz and 9.6 μmRz, respectively. The surface roughness of the floor ranges from 46 μmRz to 99 μmRz depending on the measurement position.

Using the stiffness model described in Section 2.1, the stiffness of each support is calculated from the five components shown in Fig. 15. The contact stiffness is

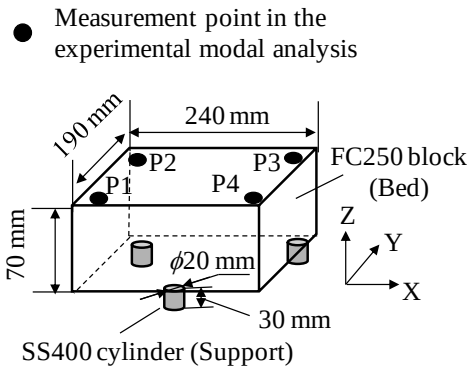

Fig. 13 Model of a machine tool bed

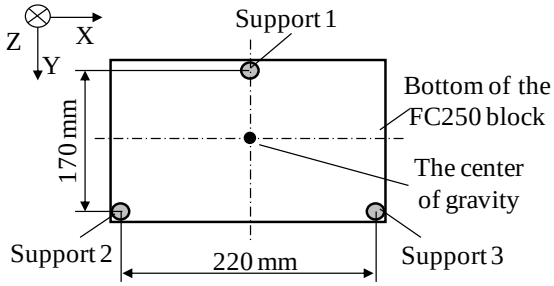

Fig. 14 Position of supports

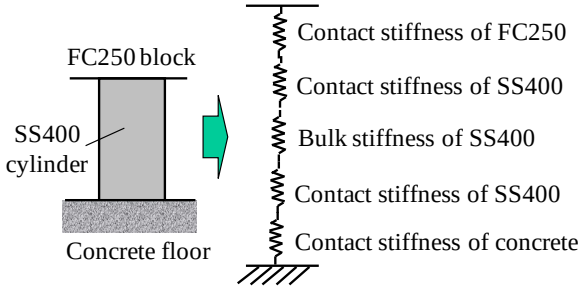

Fig. 15 Stiffness model of supports

Table 3 Estimated stiffness of supports

	Normal direction		Tangential direction	
	Support 1	Supports 2 and 3	Support 1	Supports 2 and 3
Contact stiffness of FC250 N/mm	6.3×10^5	3.1×10^5	1.3×10^5	6.6×10^4
Contact stiffness of SS400 N/mm	1.1×10^6	5.6×10^5	1.0×10^5	5.0×10^4
Bulk stiffness of SS400 N/mm	2.2×10^6	2.2×10^6	1.8×10^5	1.8×10^5
Contact stiffness of SS400 N/mm	3.6×10^6	1.8×10^6	3.2×10^5	1.6×10^5
Contact stiffness of concrete N/mm	6.6×10^4	3.3×10^4	4.3×10^3	2.2×10^3
Total stiffness of the support N/mm	5.5×10^4	2.8×10^4	3.9×10^3	2.0×10^3

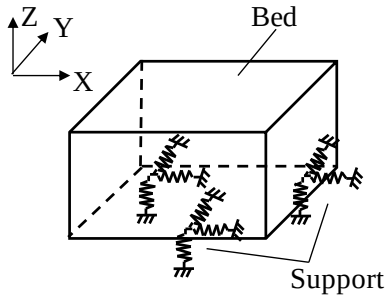

Fig. 16 Rigid body model used in the estimation

calculated from the normal preload and the unit contact stiffness. The unit contact stiffness given in Section 3 is used. The bulk stiffness is determined using analytical formulas of the axial stiffness and bending stiffness of a cylinder. Table 3 lists the calculated values. For both normal and tangential directions, the contact stiffness of concrete is found to be less than 1/10 of the others and primarily determines the overall stiffness of the supports.

4.2 Method of vibration mode shape analysis by estimation and experiment

The rigid body model is used to estimate the natural frequency and vibration mode shape. Figure 16 shows the developed model. The block is approximated by a rigid cuboid with six degrees of freedom. The block is coupled to the inertial system by three 3D stiffnesses corresponding to the supports. The calculation is conducted with a software for rigid body simulation, Axis Construction Kit [16].

An impulse hammer (PCB Piezotronics) is used to conduct an impact test to experimentally analyze the vibration mode shape. The block is excited at its center in the Y and Z directions. To obtain a 3D vibration mode shape, a 3D accelerometer (PCB Piezotronics) is used to measure the acceleration at four corners, P1-P4, shown in Fig. 13. The frequency response between the excitation force and acceleration is computed with a portable FFT-analyzer (Ono Sokki). Then, the frequency response between the excitation force and displacement is obtained by integration. The sensitivities of the impulse hammer and the accelerometer are 2.3 mV/N and 50 mV/m/s^2, respectively. The measurement frequency range is set to 500 Hz, and the number of sample points is 2048. The number of averaging is five.

4.3 Experimental result

The measured frequency responses between the excitation force and displacement are shown in Figs.17 and 18. In Fig.17 which shows the result in the Y direction, three resonance peaks are observed at 60 Hz, 83 Hz, and 117 Hz. In Fig.18 which shows the result in the Z direction, two resonance peaks are seen at 312 Hz and 382 Hz. These five resonance peaks correspond to the first five vibration modes of the model.

4.4 Comparison of experimentally measured and estimated vibrations

Table 4 presents a comparison of the natural frequency and vibration mode shape of the first five vibration modes. In the table, the natural frequencies estimated considering only the bulk stiffness of the support are also shown for comparison. Although the

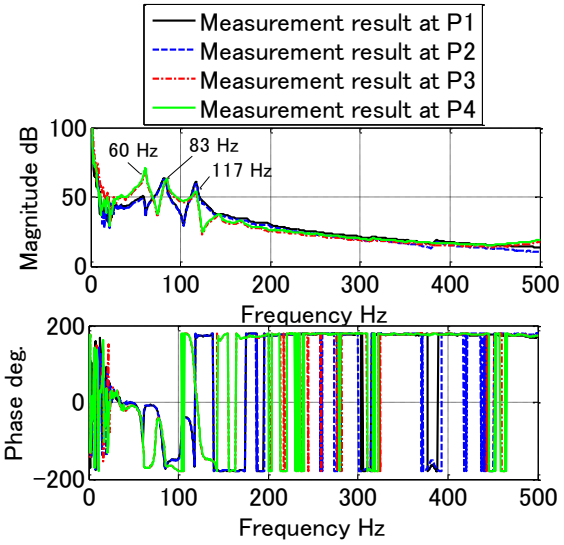

Fig. 17 Frequency response between the excitation force in the Y direction and the displacement in the Y direction

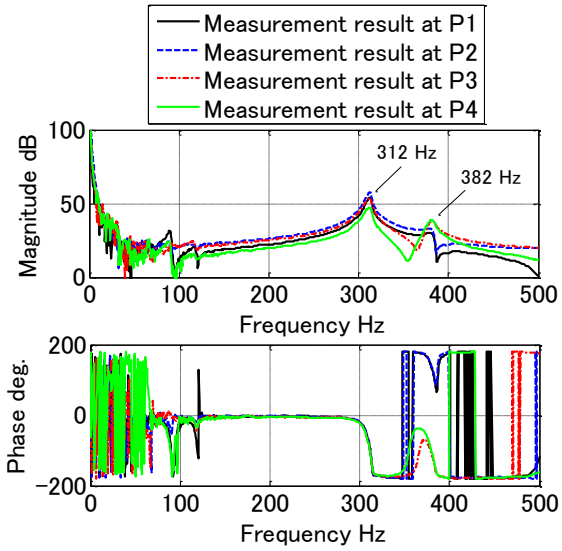

Fig. 18 Frequency response between the excitation force in the Z direction and the displacement in the Z direction

Table 4 Comparison of natural frequency and vibration mode shape

Mode No.	Estimation with the proposed model		Experiment		Estimation considering only the bulk stiffness
	Natural frequency Hz	Mode shape description	Natural frequency Hz	Mode shape description	Natural frequency Hz
Mode 1	93	Translation in the X direction	60	Translation in the diagonal direction in the XY plane	729
Mode 2	93	Translation in the Y direction	83	Translation in the diagonal direction in the XY plane	765
Mode 3	122	Rotation around the Z direction	117	Rotation around the Z direction	1104
Mode 4	350	Translation in the Z direction	312	Translation in the Z direction	2444
Mode 5	381	Rotation around the Y direction	382	Rotation around the Y direction	3377

natural frequency considering only the bulk stiffness is almost 10 times that of the experimental value, the estimation with the proposed model is comparable to the experiment.

The difference in the vibration mode shapes of modes 1 and 2 can be attributed to two factors. The first is that the normal load distribution was uneven due to the flatness of the concrete floor, which caused the normal preload on Support 2 to be less than those on supports 1 and 3. In order to verify the effect of the normal load distribution, the support should have a function to measure the normal load. The second is that the concrete of the specimen of Section 3 was not the same as that of the floor of Section 4. In the light of this, and considering that the contact properties of the floor differ from place to place, it would be necessary to consider the unit contact stiffness of the floor of the particular workshop in which a machine tool bed is to be installed.

The observations of the experiment show that the contact stiffness of the supports significantly determined the vibration of the block. The normal preload of the experiment was less than what is usually encountered in actual cases because the mass of the block model was less than that of real machine tool beds. Consequently, the influence of the contact stiffness in the experiment was greater than what is obtained in actual cases. However, even if the mass of the experimental block had been 100 times that of what was used, the contact stiffness of the concrete floor could not be ignored, since it would still be equal to the bulk stiffness (see Table 3). On the basis of the results of this study, it is proposed that the contact stiffness between the supports of a machine tool bed and the concrete floor primarily determines the vibration properties of the machine.

5. Conclusions

A 3D stiffness model of a machine tool support was proposed in this study using contact stiffness. The stiffness in each direction was assumed to be determined by the contact stiffness at the interfaces and the bulk stiffness between the supports and the floor. The contact stiffness model proposed by Shimizu et al. was expanded to determine the contact stiffness in the normal and tangential directions of an interface. In the proposed model, the contact stiffness is obtained by multiplying the unit contact stiffness by the real contact area. The contact stiffness of concrete was experimentally investigated to estimate the stiffness between machine tool supports and the floor, and it was observed to be the primary determinant of the stiffness of interfaces between metal and concrete. Moreover, the unit contact stiffness of concrete was discovered to be less than 1/10 of those of the metals that were used for the study. The natural frequency and vibration mode shape of a model machine tool bed were also experimentally measured and used to verify the proposed stiffness model. The comparison of the results obtained from the two procedures showed that the natural frequency and vibration mode shape of a machine tool bed can be predicted using the proposed stiffness model.

Acknowledgements

This work was supported by Mazak foundation and KAKENHI (24760104).

References

[1] Eugene I.Rivin: Vibration isolation of precision equipment, Precision Engineering 1995;17:41.

[2] C.F.J.Geerts, G.H.Veldhuizent: Precision copying machine for variable curvature surfaces, Precision Engineering 1984;6:9.

[3] D.C.Thompson, J.L.Chrislock, L.E.Newton: T Development of an inexpensive, high accuracy diamond turning machine, Precision Engineering, 1982;4:73.

[4] Tomonori Kato, Kenji Kawashima, Tatsuya Funaki, Kotaro Tadano, Toshiharu Kagawa: A new, high precision, quick response pressure regulator for active control of pneumatic vibration isolation tables, Precision Engineering, 2010;34:43.

[5] T.Hoshi: Chatter Vibration in Machining -Analysis and Countermeasure-, Kogyo Chosakai Publishing Co., Ltd., Tokyo, 1977, pp.210-227.(in Japanese)

[6] K.Yoshida, H.Shimura, H.Yahagi, J.Yoshioka: Effects of mounting elements of surface grinding machines upon their relative receptances between grinding wheel and work table, Journal of mechanical working technology 1988;17:377.

[7] R.D.Mindlin: Compliances of elastic bodies in contact, Journal of applied mechanics 1949;16 :259.

[8] J.A.Greenwood, J.B.P.Williamson: Contact of nominally flat surfaces, Proceedings of royal society London 1966; A295:300.

[9] Hany.A.Sherif, S.S.Kossa: Relationship between normal and tangential contact stiffness of nominally flat surfaces, Wear 1991;151:49.

[10] Masatoshi Hashimoto, Etsuo Marui, Shinobu Kato: Estimation of contact stiffness at interfaces in machine structures by a beam model on an elastic foundation, Tribology international 1994;27:423.

[11] M.Gonzalez-Valadez, A.Baltazar, R.S.Dwyer-Joyce: Study of interfacial stiffness ratio of a rough surface in contact using a spring model, Wear 2010;268:373.

[12] R.H.Thornley, R.Connolly, M.M.Barash, F.Koeningsberger: The effect of surface topography upon the static stiffness of machine tool joints, International journal of Machine tool design and research 1965;5:57.

[13] Shinji Shimizu, Kyoko Nakamura, Haruhisa Sakamoto: Quantitative Measurement method of contact stiffness of the joint with different material combination, Journal of advanced mechanical design systems and manufacturing 2010;4:1044.

[14] F.P.Bowden, and D.Tabor: The Friction and Lubrication of Solids, Oxford , 1954, (Translated by N.Soda, Maruzen Company Ltd., Tokyo, 1961), pp.9-17.

[15] D.Kono, T.Inagaki, A.Matsubara, and I.Yamaji: Measurement of contact stiffness for stiffness estimation of machine tool supports, Key Engineering Materials 2012; 523-524:457, Proceedings of the 14th International Conference on Precision Engineering (ICPE 2012).

[16] Th. Lorenzer, S.Weikert, S. Bossoni and K. Wegener: Modeling and evaluation tool for supporting decisions on the design of reconfigurable machine tools, Journal of Manufacturing Systems 2007;26:167.

List of Figure Captions

Table 1 Specifications of measuring instruments

Force sensor	Measuring range	±5 kN
	Accuracy	±1%
Load cell	Measuring range	±10 kN
	Accuracy	±0.02%
Capacitive displacement sensor	Measuring range	±250 μm
	Accuracy	±1%

Table 2 Specifications of specimens

Material	S50C	SS400	FC250	Concrete
Longitudinal elastic modulus GPa	205	206	127	25–40
Measured Vickers hardness kgf/mm^2	230	180	230	56 (mortar) 1470 (gravel)
Measured surface roughness Rz μm	4.0	1.1	1.5	3.6
Unit normal contact stiffness δk_n N/mm/mm^2	1.4×10^7	1.8×10^7	1.0×10^7	Not measured
Unit tangential contact stiffness δk_t N/mm/mm^2	1.6×10^6	1.6×10^6	2.0×10^6	Not measured

Table 3 Estimated stiffness of supports

	Normal direction		Tangential direction	
	Support 1	Supports 2 and 3	Support 1	Supports 2 and 3
Contact stiffness of FC250 N/mm	6.3×10^5	3.1×10^5	1.3×10^5	6.6×10^4
Contact stiffness of SS400 N/mm	1.1×10^6	5.6×10^5	1.0×10^5	5.0×10^4
Bulk stiffness of SS400 N/mm	2.2×10^6	2.2×10^6	1.8×10^5	1.8×10^5
Contact stiffness of SS400 N/mm	3.6×10^6	1.8×10^6	3.2×10^5	1.6×10^5
Contact stiffness of concrete N/mm	6.6×10^4	3.3×10^4	4.3×10^3	2.2×10^3
Total stiffness of the support N/mm	5.5×10^4	2.8×10^4	3.9×10^3	2.0×10^3

Table 4 Comparison of natural frequency and vibration mode shape

Mode No.	Estimation with the proposed model		Experiment		Estimation considering only the bulk stiffness
	Natural frequency Hz	Mode shape description	Natural frequency Hz	Mode shape description	Natural frequency Hz
Mode 1	93	Translation in the X direction	60	Translation in the diagonal direction in the XY plane	729
Mode 2	93	Translation in the Y direction	83	Translation in the diagonal direction in the XY plane	765
Mode 3	122	Rotation around the Z direction	117	Rotation around the Z direction	1104
Mode 4	350	Translation in the Z direction	312	Translation in the Z direction	2444
Mode 5	381	Rotation around the Y direction	382	Rotation around the Y direction	3377

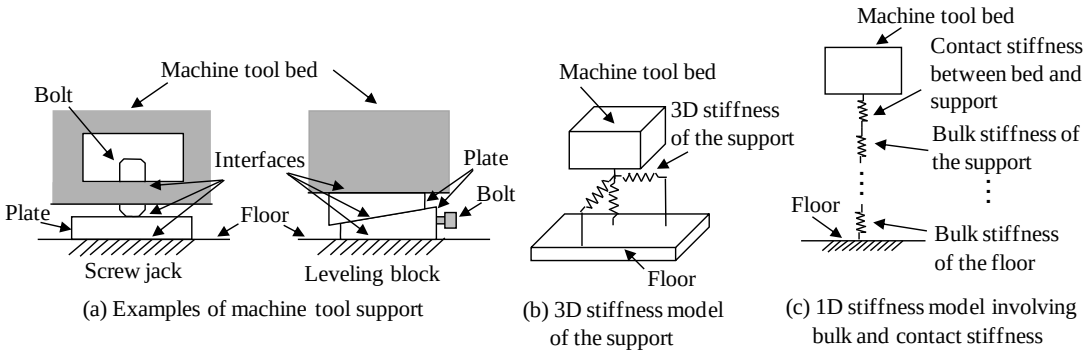

(a) Examples of machine tool support (b) 3D stiffness model of the support (c) 1D stiffness model involving bulk and contact stiffness

Fig. 1 Machine tool support and its model

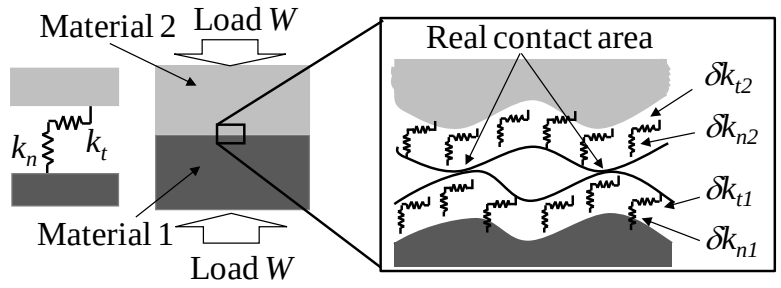

(a) Contact stiffness in the support

(b) Unit contact stiffness model at the interface

Fig. 2 Model of contact stiffness

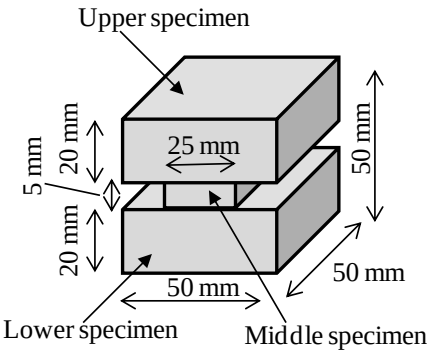

Fig. 3 Specimen set used in the measurement

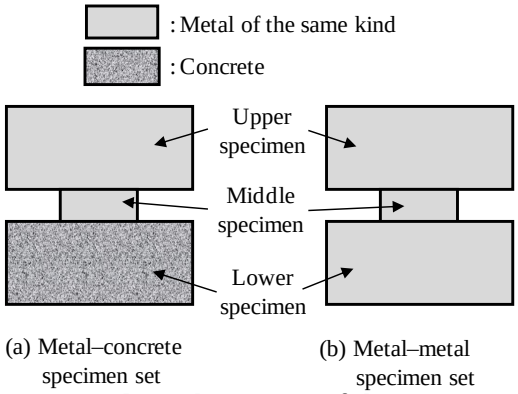

Fig. 4 Material combinations of the specimen set

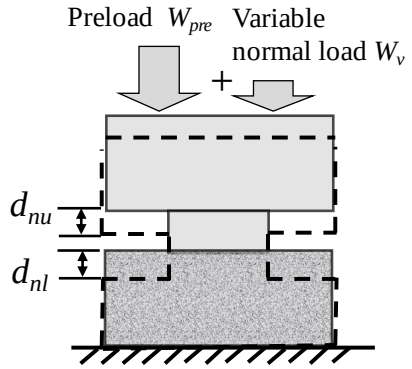

Fig. 5 Schematic of measurement in the normal direction

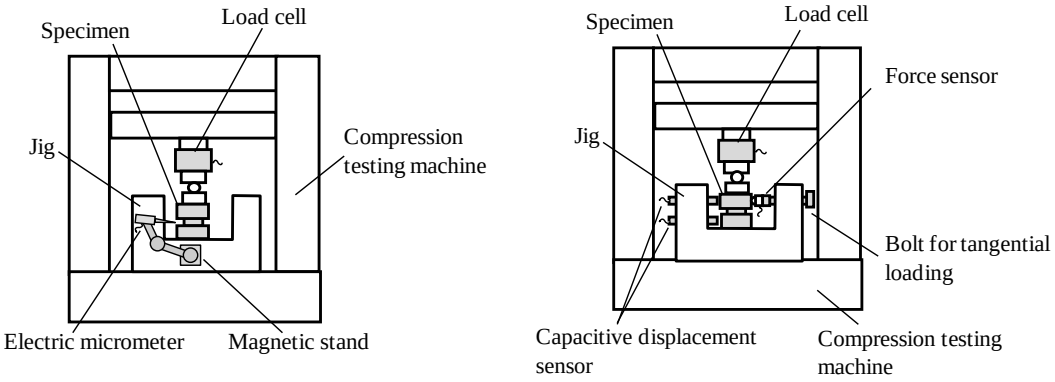

(a) Measurement in the normal direction

(b) Measurement in the tangential direction

Fig. 6 Schematic of measurement setup

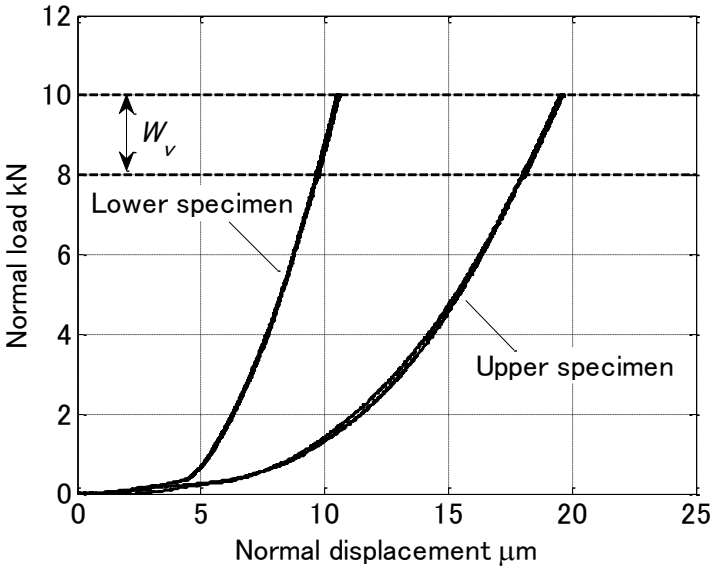

Fig.7 Relationship between normal displacement and load for the metal–concrete specimen set. The material of the metal specimen is S50C.

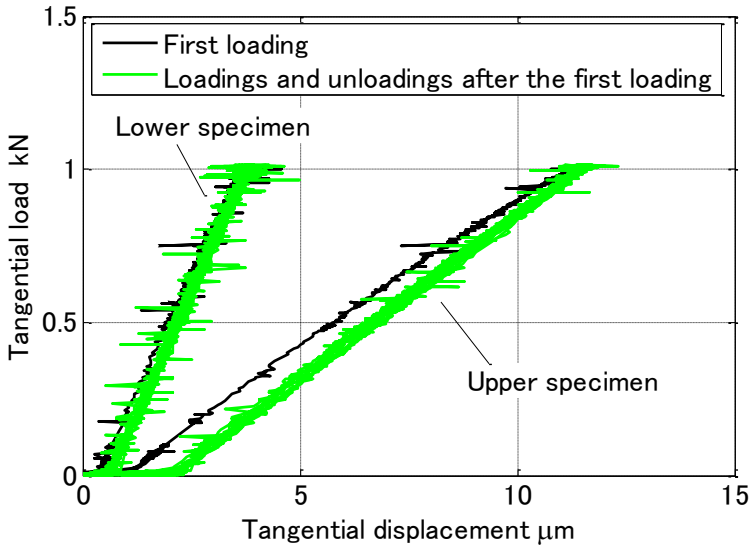

Fig.8 Relationship between tangential displacement and load for the metal–concrete specimen set. The material of the metal specimen is S50C.

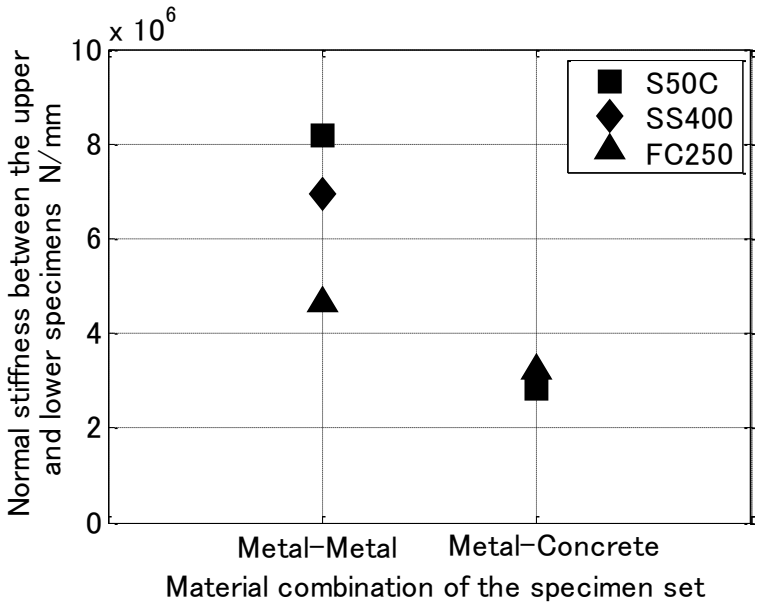

Fig. 9 Comparison of normal stiffness between the upper and lower specimens

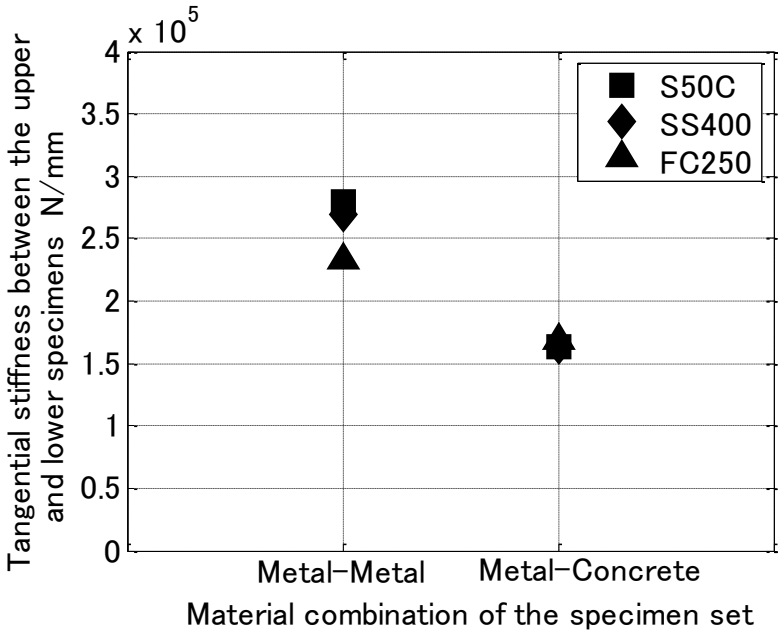

Fig. 10 Comparison of tangential stiffness between the upper and lower specimens

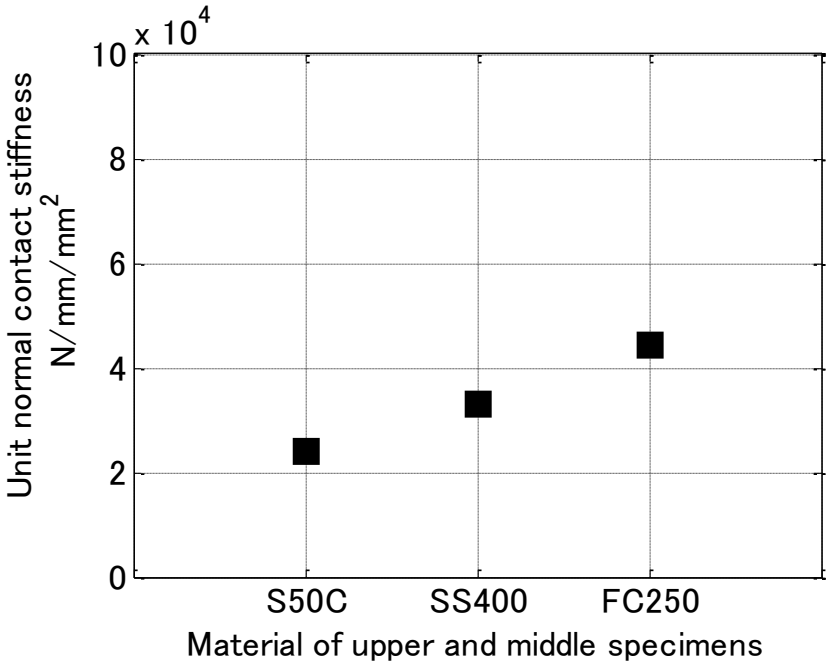

Fig. 11 Unit normal contact stiffness of concrete

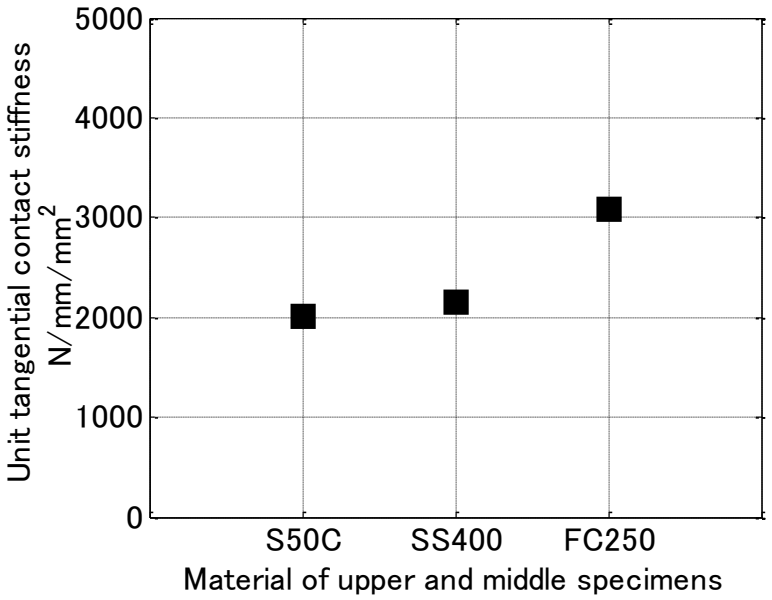

Fig. 12 Unit tangential contact stiffness of concrete

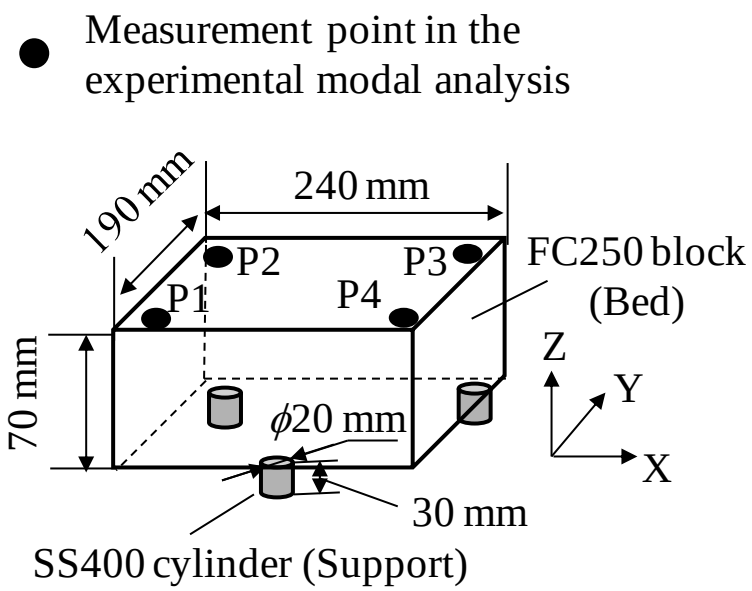

Fig. 13 Model of a machine tool bed

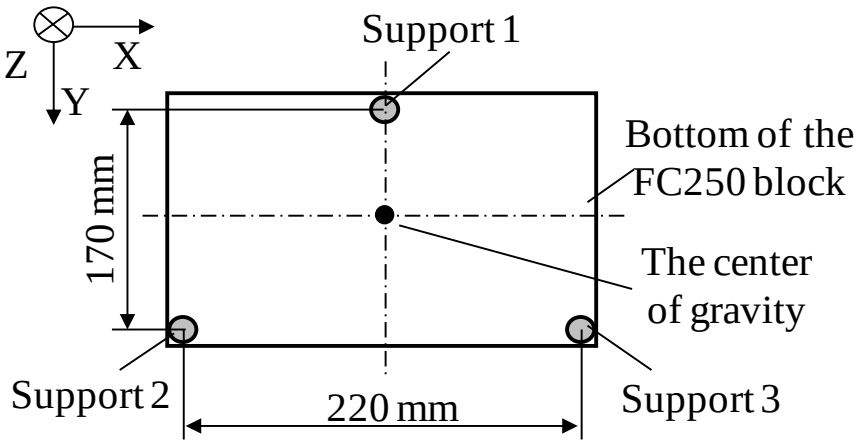

Fig. 14 Position of supports

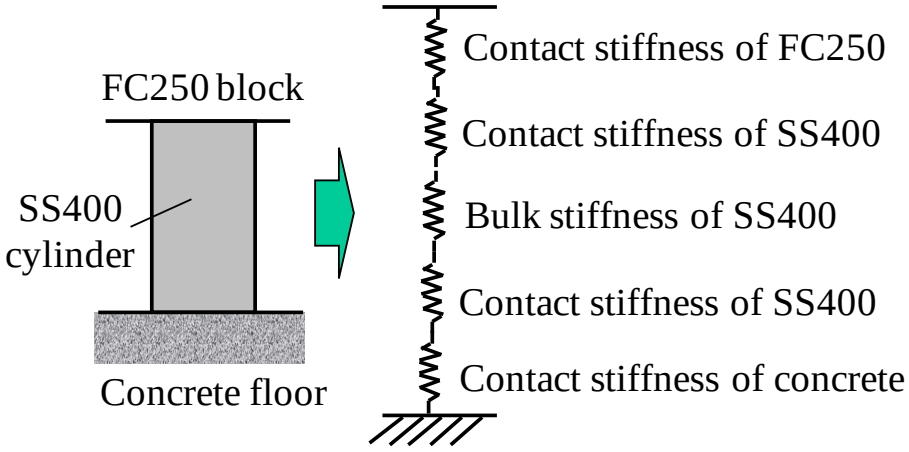

Fig. 15 Stiffness model of supports

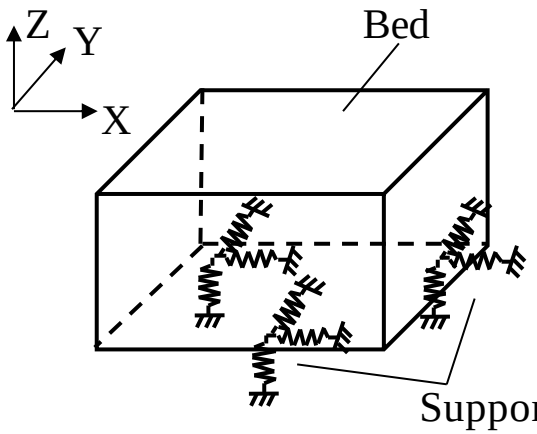

Fig. 16 Rigid body model used in the estimation

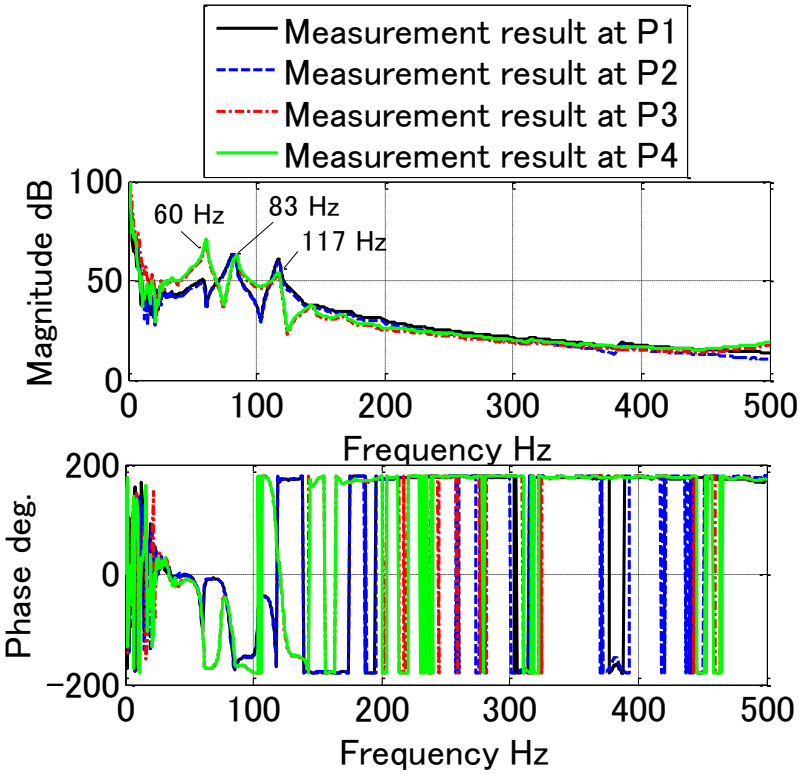

Fig. 17 Frequency response between the excitation force in the Y direction and the displacement in the Y direction

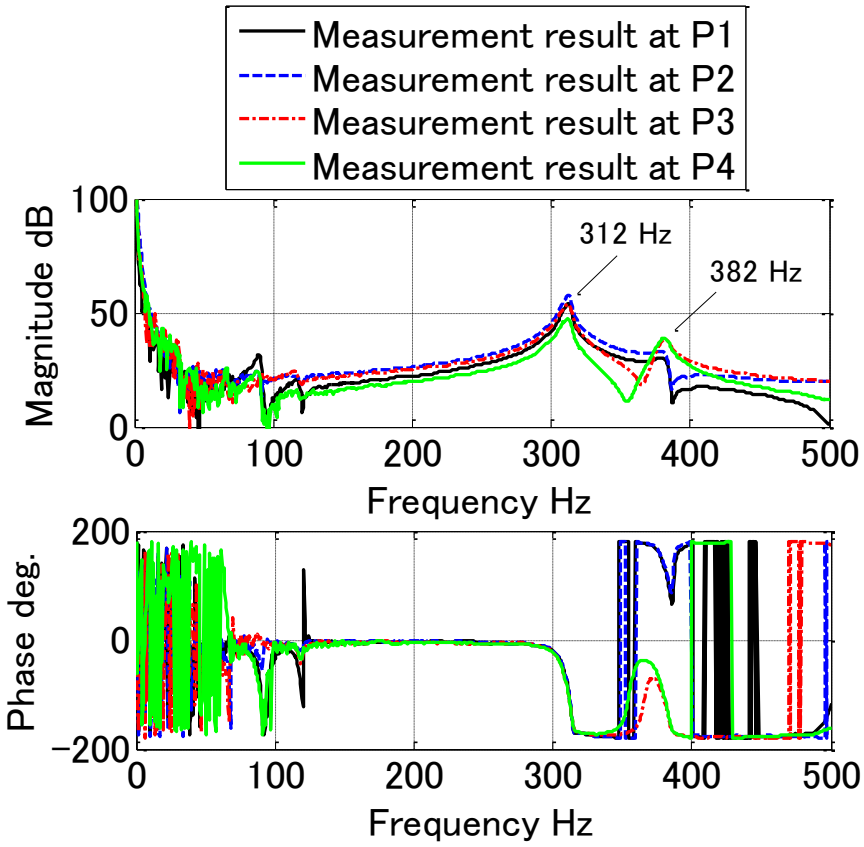

Fig. 18 Frequency response between the excitation force in the Z direction and the displacement in the Z direction